Detailed Numerical Analysis of X-ray Phase Contrast Imaging in Sprays

Mark A. Linne*
Combustion Engine Research Center, Department of Applied Mechanics
Chalmers University, Gothenburg, Sweden
mark.linne@chalmers.se

Abstract

Recent studies of spray-related flowfields using synchrotron-based x-ray phase contrast imaging (PCI) have produced results that are sometimes straightforward to interpret in terms of the fluid structure, but in other cases the images do not reflect generally accepted physics of fluid motion. It has been unclear why some images have the appearance of a normal fluid stream while others depart significantly from expectation. The detailed numerical modeling presented in this paper is meant to explain the images and resolve common questions about the technique. The simulations show that collimated x-ray beams will always contain signatures from every possible encounter, from the input plane to the exit plane, and these signatures generate overlapping phase contrast patterns that can prove at times impossible to interpret. Clouds of moderate- to large-size drops produce a complex, mottled x-ray phase contrast image that cannot be interpreted. Small drops generate something akin to one gray pixel image each, and their size is close to the resolution limit of the instrument, so the diffraction pattern is broadened by the instrument response into something more like a small diffuse gray blob. Dense clouds of small drops produce a composite image that is a fairly uniform gray mass that cannot be interpreted. Moreover, we show that it is not possible to image intact liquid structures behind clouds of drops. Whenever a meaningful number of drops is present, therefore, x-ray PCI images are dominated by unavoidable artifacts of the technique.

Introduction

Figure 1 depicts a transparent diesel fuel injector tip that was used to observe cavitation inside one hole of the tip, using microscopic shadowgraphy [1]. One can see a small stream of cavitation bubbles inside the hole and leading to the nozzle exit. Note what happens once the jet exits the hole. The fact that the spray (consisting of droplets on the order of 5 – 10 μm diameter) does not instantaneously spread indicates that many of the larger liquid structures visible inside the hole must still exist outside of the hole, as intact liquid structures undergoing primary breakup within the droplet cloud. These structures were hidden from view by the camera, however, because the droplet cloud was very dense and the density of this region has presented a significant measurement challenge to classical optical techniques.

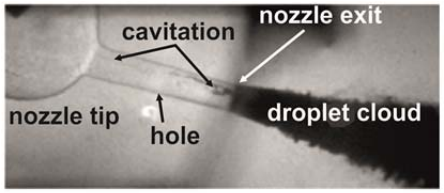

Figure 1 Microscope shadowgram of flow inside an optical diesel nozzle tip (reproduced with permission [1]*).*

Within the last decade, two very different approaches to this challenge have been proposed, developed, and discussed. One of them is ballistic imaging (BI [2]); a laser-based (optical) technique developed by the author and his group. The second approach is to use x-ray radiation. A research group at the Advanced Photon Source (APS) at Argonne National Laboratory has applied their high brightness synchrotron source to spray studies [3-11]. The stated goals of the x-ray program are to provide "quantitative data regarding fuel distribution" [10] (e.g. fuel mass) and to "visualize the near-nozzle morphology (~ 6 mm) and to better understand the primary breakup process" [11]. The APS group has reported extensively on x-ray absorption ("radiography") in various kinds of sprays. That work is discussed in a companion article to this one [12].

The APS group has also used phase contrast imaging (PCI) [13-17], with the goal to improve spatial and temporal resolution of x-ray imaging. The physical implementation of x-ray PCI is quite similar to shadowgraphy, wherein a collimated x-ray beam directly illuminates the spray. The phase changes in the x-ray wave fronts caused by interfaces as the beam crosses the spray are imbedded in the beam. At the APS, the x-ray phase contrast image is then converted into visible light in a scintillator (a thin YAG:Ce crystal) and that is imaged onto a CCD camera. The PCI technique developed for sprays at APS typically uses a short pulse of x-ray radiation at around 13.3 keV (wavelength around 0.09 nm)[1], allowing acquisition of single shot images of a transient Diesel spray with good temporal resolution [17, 18]. Phase contrast imaging has also been used to observe effervescent sprays [18] and to acquire successive images in a gasoline direct injection (GDI) spray [14, 17]. There

* Corresponding author: mark.linne@chalmers.se

[1] Note that in the x-ray regime we use photon energy ($E = hc/\lambda$) to describe wavelength of light; where h is Planck's constant, c is the speed of light in vacuum and λ is the wavelength.

are unusual aspects in the x-ray phase contrast images of sprays, however, and common questions about those features were the impetus for the modeling project described here.

Most researchers in the spray community use optical techniques with wavelengths in the visible spectrum (including near UV and IR light, all of those techniques are termed 'optical' here). In comparison, the radiation used for phase contrast imaging in sprays has a wavelength around 0.09 nm (13.3 keV; hard x-rays). If we consider a 10 μm diameter drop of fuel, then to scale the x-ray case up to visible radiation at 550 nm would mean a very large and green optical beam would be interacting with a 6 cm diameter liquid sphere. In such a case the sphere would be a large ball lens, focusing collimated light to a tight spot. That doesn't happen in the x-ray case, however, because the index of refraction at this wavelength is also very different. At 13.3 keV, the real index of the fuel is $n_{fuel} = (1 - 0.90 \times 10^{-6})$ (written in the format used in the x-ray community); it is very nearly one. At the same photon energy, the real index for air is $n_{air} = (1 - 1.41 \times 10^{-9})$; also very nearly one and actually larger than the fuel index. This means the x-ray beam passing through a 10 μm drop experiences only about 0.1 wave shift on the droplet centerline. Visible light passing through a 10 μm drop experiences around 25 wave shifts, because fuel has an index of refraction on the order of 1.3 to 1.5 at optical wavelengths. In contrast to optical wavelengths, x-ray radiation is only very slightly diffracted by a drop. It is not deviated and it scatters *very* weakly. This point is emphasized as a significant advantage in almost every article on the topic of x-ray diagnostics for sprays; within the operating range of the instrument the drops do not scatter the x-ray radiation.

The literature also emphasizes that an x-ray phase contrast image contains just signatures arising from strong index gradients (and hence gradients in the phase fronts). Such an image represents just the edges of objects. Fuel sprays are distributed collections of hundreds of droplets; many drop edges are encountered as the beam passes through the spray. Because an x-ray beam does not scatter strongly, the collimated beam will contain the signatures of absolutely every edge that stood in the beam path from the input to the exit planes, summed up at the scintillator. Later on we will discuss what this means in terms of the images that are generated.

In this paper we discuss x-ray phase contrast images presented in three articles; Wang et al. [14], Lin et al. [18], and Moon et al. [19] because they represent the range of issues under discussion here. The distance from the spray to the scintillator crystal (denoted by the letter *D*) is an important factor affecting image quality. It was reported only in the first case (Wang et al. [14]), where it was optimized for best image contrast; the “optimized defocus value for Fresnel propagation contrast and spatial resolution” was chosen. A simple explanation is that when the scintillator is too close to the object (spray) the Fresnel diffraction patterns have not fully developed (in a simple-minded geometric sense, one can think in terms of small angles not being detectable until some distance away from the source). In this case Fresnel diffraction forms the image, not a lens. As the scintillator is moved away, the patterns become well defined but beyond that point image blurring caused by the size of the illumination source and other imaging system imperfections reduce contrast (see e.g. [20]). Cloetens et al. [21] describe a simplified Fourier optics approach to optimum contrast which does not include the more complicated, long-distance blurring effects. They present a scaling argument for *D* that indicates it should be on the order of 55 cm for small spray features. Larger features image better at longer *D*, but blurring effects can take over at some point. The *D* = 70 cm value quoted in reference [14] is thus a good compromise. During discussions at conferences, the idea of adjusting *D* has been mentioned. For models, therefore, we assume the nominal value for *D* is 70 cm, but in a few cases the effect of increasing *D* is also analyzed.

Methods

To model fully the interaction between an x-ray beam and a spray requires solution of the electromagnetic formalism for light propagation [21] because phase contrast imaging relies upon wavefront interactions with media. The simulations presented here have been performed, therefore, using a commercially available code named General Laser Analysis and Design (GLAD), a physical optics code that numerically propagates an electromagnetic wave. The code provides solutions to the full diffraction problem as described by Lawrence [22]. The method is discussed in more detail by Linne [23].

The simulation propagates x-ray radiation at 13.3 keV photon energy through a sample (bubble, single drop, or collection of drops) followed by propagation through air out to *D* = 70 cm (unless otherwise stated). A flat-topped (‘super-Gaussian’) beam profile is assumed (the beam diameter is adjusted to accommodate each problem). The simulated beams are smaller than the x-ray beam used at APS but we ensure for each evaluation that the super-Gaussian profile is sufficiently large to avoid interaction between the beam edges and the drop or bubble edges. Because memory allocation is an issue for a desktop computer, such simplifications are used when they have no impact on the outcome.

Two spectral cases are evaluated throughout. In what is called the “5-beam” solution, the beam was assumed to be composed of five collinear beams with wavelengths of 0.0935, 0.0932, 0.093, 0.0928, and 0.0925 nm. All five beams were propagated independently and then incoherently summed at *D* to simulate a broadband beam (this represents a top-hat, 5-mode spectral profile with the same full-width at half-maximum as the real beam). A beam with just five infinitely narrow modes is not as broadband as the real beam, but it will allow us to assess

the importance of bandwidth. A single beam at single wavelength of 0.093 nm (a "1-beam" solution) is sometimes propagated, to evaluate bandwidth effects and for other reasons given below.

Simulations for a beam that propagated through single drops of diameter 80, 30, 10 and 5 μm (and sometimes other sizes) have been performed because the various studies of interest have covered that same drop size range. For the large drops, the spatial resolution of the imaging system does not play a serious role, but for the small drops the drop diameter falls into the same order of magnitude as the spatial resolution of the system. As an example, Wang et al. [14] quote a resolution between 5 and 30 μm, and in this case small-drop images will always be blurred. The spatial resolution of the system was modeled here in some cases by smoothing the synthetic images with a Gaussian filter function that had the same width as the quoted resolution in the article under evaluation.

Results and Discussion

Figure 2 contains cross-sectional beam images (imitating the format of the experimental PCI images) for propagation of a 100 μm beam through a single 80 μm feature (drop or bubble) followed by propagation 70 cm in air. The index difference used was that of fuel and air. Image 2a. is for a drop, and it was produced by the 5-beam solution. As a reference, the same simulation using the 1-beam solution is included as Figure 2b. One can see that the 1-beam solution produces more fine diffractive structure than the 5-beam solution does. This is an expected outcome, given the infinitely narrow bandwidth of such a single frequency solution. Even the 5-beam solution contains more fine structure than experimental images, however. This happens because the real x-ray beam is not coherent. The large diffraction structures remain the same, however, even when the fine features begin to be washed out by bandwidth (e.g. compare Figure 2b. to Figure 2a.). It is the large features that matter for this simulation. In Figures 2c. and 2d. we present corresponding images for bubbles. A change in index difference causes the dark and light rings to switch places. The ability of x-ray PCI to differentiate between a drop and a bubble is often emphasized in articles that use this technique.

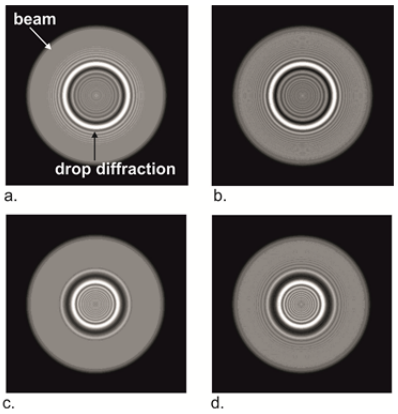

Figure 2. PCI of an 80 μm drop or bubble in a 100 μm x-ray beam.

Figure 3 presents images produced by the 5-beam solution for droplet sizes ranging from 80 μm (Fig. 4a.), to 30 μm (Fig. 4b.), to 10 μm (Fig. 4c.), to 5 μm (Fig. 4 d.). Here D was set to 70 cm and the super-Gaussian beam width was 100 μm. Note how the diffraction band changes as a fraction of the drop diameter. Figures 3c. and 3d. are for small drops, and the diffraction band has closed into the center of the pattern; the image that is impressed upon the x-ray beam is similar to a single gray pixel. Small drops produce small gray dots under these conditions.

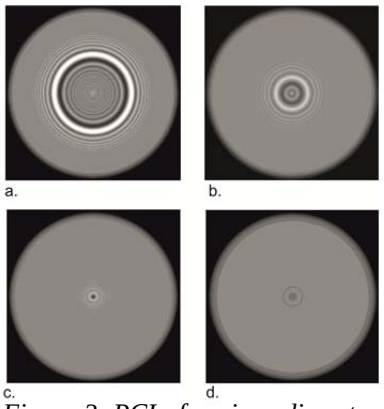

Figure 3. PCI of various diameter drops.

The experimental images of single drops and bubbles in Figures 7 - 10 of Lin et al. [18], for example, are nearly identical to the results for the large drops in Figures 2 and 3. The most notable difference is that simulations produce perfectly round images while real drops and bubbles are not necessarily round. As mentioned, the simulations also include more fine structure because they have narrower bandwidth, but the large structures match experiments, and it is those features we emphasize. While there are small differences between the simulations and the experiments, they are easily explained and they do not affect the final conclusions of this work. Linne [23] also demonstrates that the patterns produced by the 1-beam and the 5-beam solutions grow more alike as the drop size shrinks. One can use the 1-beam solutions for small drops. When we simulate a fog of small drops we will need to use a 1-beam solution to conserve memory.

Next we investigate what happens if the scintillator crystal is moved out significantly. We include solutions for 10 μm and 80 μm diameter drops at distances D of 1 cm, 1 m and 5 m in Figure 4. The 10 μm drop results are shown in Figures 4a, b, and c, where the super-Gaussian beam was expanded to 180 μm to allow image growth with distance. The 80 μm drop results are shown in Figures 4d, e, and f, where the super-Gaussian beam was expanded to 200 μm. In the D = 1 cm cases for both drops, one can see clearly the point made earlier about requiring some distance past the object to develop fully the diffraction pattern. Neither of the D = 1 cm images contains a true diffraction pattern, rather they indicate faint mode structure that will evolve into the necessary pattern with distance. As expected, the pattern for a small drop develops more quickly than that of a large drop. The D = 1 m images are not very different from the 70 cm images in Figures 2 and 3 (remembering that the simulated super-Gaussian beam diameter is now larger). This point is not surprising because once established, the diffraction patterns do not evolve quickly. The D = 5 m images demonstrate that the patterns do actually

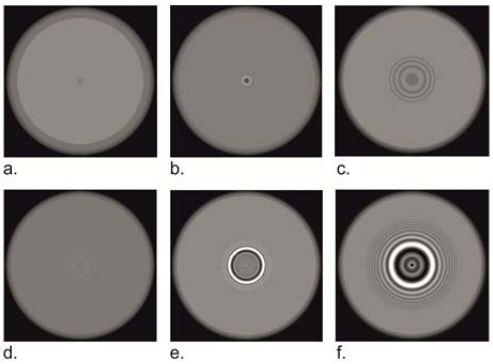

Figure 4. Effect of D; a, b & c for a 10 μm drop and d, e and f for an 80 μm drop.

evolve with distance, but, again, not very much. The divergence angles are on the order of micro-radians. This figure therefore demonstrates that the imprint of each drop becomes embedded in the beam; it does not change much with distance and it is persistent within the beam. Note that the image blurring effects that degrade real phase contrast systems at large *D* have not been modeled here. They would have affected the image components of Fig. 4c. and f. equally.

As a next step, two overlapping drops are investigated (Figure 5). One drop is placed just in front of the other and they are offset sideways by a small amount. One can clearly see that the two patterns mix even though the individual beam systems are added incoherently. The small drops remain gray pixels, and so their overlap produces more of a lightly speckled gray structure. Larger drops form overlapping light and dark bands that produce a more complex and much more deeply modulated (light and dark) structure. The differences between Figures 5a., b., and c. go a long way towards explaining differences between x-ray PCI images taken from sprays with large drops and those with small drops.

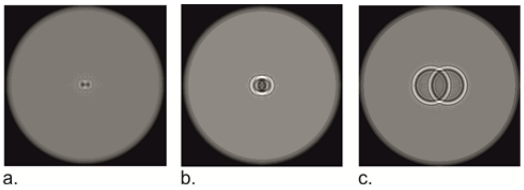

Figure 5. Two drops (one in front of the other) in a 180 μm beam at D = 70 cm; a. 10 μm drops, b. 30 μm drops and c. 80 μm drops.

Next, the most recent effervescent spray results presented by Lin et al. [18] are analyzed. One goal of the present work is to simulate the drop cloud images in that article (see e.g. Fig. 6a.). The two-drop results presented in Figure 5 begin to explain it. To simulate the flow field we used a 5-beam simulation with a 300 μm super-Gaussian x-ray beam, and the drops were water [n_{water} = (1-1.31 x10^{-6})] at 13.3 keV, to match the experiments. The result in Figure 6 were simulated two ways. First, 100 drops were placed randomly within a field that was 200 μm square. The drop sizes used for this simulation ranged between 10 and 50 μm. For each drop, the x and y positions and the drop diameter were chosen by random numbers (a flat distribution) that fell within the location and size ranges. Each drop center was also located 60 μm along the axis (z) away from the foregoing drop. Note that this drop density is extremely high, but Linne [23] has demonstrated that the total number of drop interactions controls the outcome in PCI of sprays, not drop density. Since the simulations are to be directly compared to published images, the spatial resolution of the experimental system was modeled by smoothing the synthetic images with a 2 μm Gaussian filter function. This is a fairly small number (high resolution), but the value was chosen to avoid degrading the images too much. The simulation result appears in Figure 6b. Figure 6b. does not look exactly the same as Figure 6a. because it is a synthetic result for round drops. Moreover, the synthetic image has not been manipulated in the same way as the experimental images (edges have not been sharpened and the image has not been colored). Otherwise, the point is clear. After passing through a relatively small number of drops, the x-ray beam acquires a complex, deeply modulated pattern of shapes caused by the edges of the drops that were encountered along the path. The bulk of the image cannot be interpreted to extract useful information.

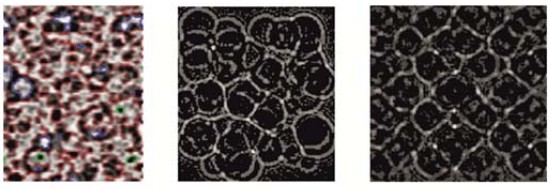

Figure 6. a. Experimental x-ray PCI, b. and c. simulations of the same image (see text).

The image in Figure 6b. took a very long time to compute. To add more drops in an efficient manner, we define a simple drop pattern that can be repeated many times using GLAD macros. Figure 6c. contains a 5-beam simulation using a 180 μm super-Gaussian beam traversing through 30 μm drops along the path. Figure 6c. was constructed using 50 plane, square grids of four drops with their centers spaced apart by 60 μm. One can see immediately that this approach provides the same conclusion that we reached with Figure 6b. One can conclude that x-ray phase contrast images of sprays with large drops appear as they do because they represent the summation of numerous drop edge interactions as the x-ray beam crosses the spray. The signatures of these interactions do not leave the beam and their contributions are summed at the scintillator crystal. Because the drops are relatively large, they produce a deeply modulated, mottled structure. The image cannot be interpreted to extract useful information. When discussing the image from which Figure 6a. was extracted, Lin et al. [18] state that the figure "shows an image taken close to the core of the spray… Here, the highly overlapping features make object identification nearly impossible and no size measurement can be made within this region." Several of the associated authors had identified this problem already in 2010. They then asserted that there are regions of this spray

that can be interrogated, but the modeling presented here indicates that such regions have low optical depth and could be interrogated via optical means as well.

To determine whether or not PCI is capable of visualizing an intact liquid structure inside the spray formation region, we simulate a large liquid structure by modeling a 150 μm drop (called the 'core drop' here) that is located behind several 4-drop arrays with spacing of 60 μm (center to center). Figure 7 contains 5-beam simulations using a 300 μm super-Gaussian beam traversing first through the core drop followed by several 4-drop arrays. The image was filtered with a 2 μm Gaussian filter. In Figure 7a. we have added only two 4-drop arrays in front of the core drop, and offset the two by 40 μm in the x and y directions. One can see the core drop structure located both inside and outside (for reference) of the 4-drop arrays. Clearly, one can detect the presence of the core drop in addition to the two arrays. The very fine diffractive structure in this and other images is a result of the relatively narrow bandwidth of this solution but it does not affect larger structures or the conclusions one can draw regarding the larger structures.

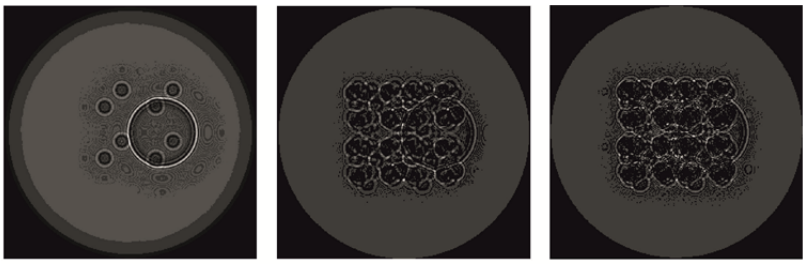

Figure 7. Simulation of intact liquid behind drops (see text).

Figure 7b. contains fifty 4-drop arrays with various offset values. In this case, 4 - 5 drops at most stand between the edge of the core drop and the scintillator. Even though the edge of the core drop can be detected, it has been corrupted significantly by the drop field and it is not clear that it could be evaluated correctly. Figure 7c. contains one hundred arrays, with eight drops at most between the edge of the core drop and the scintillator. By this time the solution has produced spatial patterns similar to Figure 6a. Once a certain number of drops has been encountered, the outcome looks the same no matter how many more are added. In Figure 7c. one can see the simulated core drop in locations where there are no other drops, but once it falls behind the drop cloud it is indiscernible. The sequence of images (from Figure 7a. to 7c.) demonstrates that somewhere between 4 and 8 drop interactions (for 30 μm water drops) is enough to obscure totally a liquid core. The idea of adjusting *D* to reveal the core has been discussed informally. The concept has been assessed here by repeating these simulations for several values of *D*, going out to 5 m. The results were not significantly different from Figure 7c. Moving the scintillator out makes no difference other than blurring the image.

Next, the article by Wang et al. [14] describes x-ray phase contrast imaging in a gasoline spray produced by single- and two-hole pressure-atomized injectors spraying into a quiescent gas at one bar (see Figure 8 for typical results). Formation of a dense droplet field at the nozzle exit was confirmed by laser shadowgraphy (e.g. Figures 8a. and c.). Several x-ray phase contrast images in reference [14] that were taken at very early times (before drops were formed) look similar to shadowgrams of a fluid flow, including image elements such as multi-scale turbulence in the core and an outer shear layer. Images taken later on (during the established spray phase, e.g. Figures 8b. and d.) are dominated by thin filament features that separate fairly uniform fields of gray. It is hard to explain how the formerly turbulent flow could have transitioned into what appears in Figures 8b. and d. Wang et al. asserted that the filaments are the edge-based signatures of “membrane-mediated breakup”, citing Lasheras and Hopfinger [24]. As explained in detail in reference [23], the membrane assertion is very difficult to credit when applied to the injector in reference [14]. If we put aside the idea of membranes, one is left with similar questions to those we asked about the effervescent spray. One goal, therefore, is to model the drop cloud to see if there is a more plausible explanation for the structures in Figures 8b. and d. A second goal is to answer the question of whether or not the technique is capable of imaging a larger structure (e.g. possibly a liquid core) that is embedded well inside the drop field.

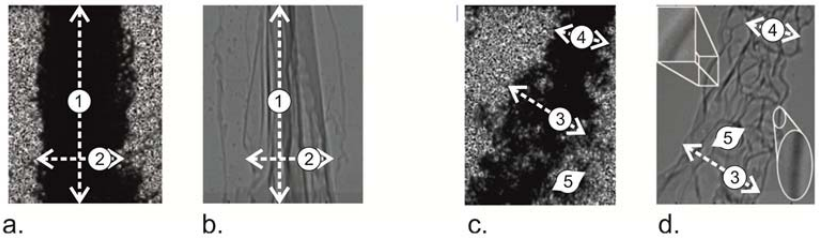

Figure 8. Results from reference [15] (reproduced with permission).

The laser shadowgrams indicate that a dense cloud of drops was present. Therefore, a fixed drop diameter of 7 μm (characteristic of these kinds of gasoline sprays) has been chosen for this simulation. The exact drop size is not as important as the fact that the drops did not produce the highly modulated patterns characteristic of large drops, as discussed just above. That much is clear from the images. A drop diameter of 7 μm will produce the alternative, gray pixel patterns.

The approach to simulation of this problem is somewhat different because the drops are small and numerous. Such small drops cannot be represented by regular arrays, as was done above. The spatial frequencies of the regular arrays end up producing artificial, repeating patterns that dominate the synthetic image, no matter how many arrays are used and no matter if the arrays are placed randomly. It was thus necessary here to randomly locate individual drops. As mentioned above, however, it is possible to use a 1-beam solution with small drops and that provides memory savings. Square planes of drops (150 μm per side) were used, and 50 drops were randomly located in each plane (in x and y). Each of the planes was then spaced 10 μm away from the foregoing plane (along z). Again, drop density does not affect the x-ray simulation.

A 300 μm beam was propagated through and around this field of drops. Wang et al. used Viscor 16-A (a surrogate gasoline), modelled here as a normal hydrocarbon fuel. We apply a spatial resolution of 15 μm (in the middle of the reported range). Figure 9 presents results for a case with six planes of drops and nothing else. This situation produces a much more uniform gray mass when compared to similar results for large drops (Figure 6), and this difference is consistent with experimental results. The only differences between the image in Figure 8b. and the simulation in Figure 9 are the filaments. We address that issue next.

Figure 9.

Consider the spatial scales of the images (not the flow scales, consider just the image spatial scales as denoted by the white arrows) in Figure 8. The arrows used in Figure 8b. are directly copied and pasted from Figure 8a., and the arrows in Figure 8d. were also copied and pasted from Figure 8c.; their lengths and orientations were not changed. Note how both Figures 8a. and 8b. have an elongated scale in the vertical dimension (vectors number 1) and a single characteristic width (vectors number 2). The image scales are exactly the same in the two images. Both Figures 8c. and 8d. are markedly different from Figures 8a. and 8b., but they are different in exactly the same way with respect to their image spatial scales (which are identical in c. and d.). The implication is that the drop clouds in Figures 8a. and 8c. could potentially be determining the image spatial scales of the filament structures in Figures 8c. and 8d. The hypothesis, therefore, is that edges of drop clouds might be imaged as the unusual filaments in the PCI; clouds can form steep droplet concentration gradients and when the drop size falls below the spatial resolution of the instrument it is not possible to differentiate between membrane edges and drop cloud edges. One could imagine, as one example, an outer cloud rolling up, and that cloud would have a distinct edge located in space some distance from the main spray body and normal to the x-ray beam. Indeed, the image in Figure 8c. hints at this. This hypothesis has been tested by adding six new planes of drops spaced just past the original planes that produced Figure 9. The most important point is that the second collection of planes has a well-defined vertical edge of drops at the center (x = 0) of the original cloud. The second drop cloud was spaced 50 μm past the first drop cloud, and it had a drop cutoff in a vertical line crossing the center of the drop cloud. As before, a 15 μm Gaussian spatial filter was applied. The simulation result is presented in Figure 10a. and a similar sized region from Figure 8b. has been copied and included here (Fig. 10 b.) for comparison. One can see that the two are quite similar. Steep droplet concentration gradients at edges of drop clouds could explain the filaments. This result does not prove that the drop clouds are the source of these image features, but it does demonstrate that drop distributions can produce such features. This explanation is consistent with the image spatial scales as highlighted in Figure 8; it is plausible and self-consistent. An explanation based on membranes buried within the drop cloud is physically untenable [23].

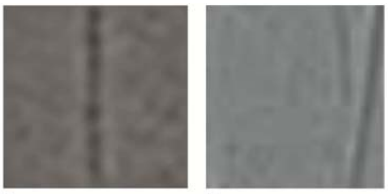

a. b.

Figure 10. a. Simulated filament structure, b. actual filament.

It is also necessary to investigate whether or not x-ray PCI is capable of imaging a larger structure that is embedded well inside a drop field such as this one. Similar to aerated spray, we simulate an intact liquid structure by modeling a 150 μm core drop. It was located behind a cloud of 7 μm diameter droplets in a similar arrangement the scheme that produced Figure 9. Figure 11 contains 1-beam simulations using a 300 μm super-Gaussian beam. The images in Figure 11 were smoothed with a 15 μm filter. Figure 11a. presents a case of 24 planes with fifty drops each (1,200 drops), and there were about 4 - 6 drops standing between the edge of the core drop and the scintillator. Similar to Figure 7b. the core drop is still discernible, but it has been corrupted significantly by the drop field and it is not clear that it could be evaluated correctly. Figure 11b. presents a case of 48 planes with fifty drops each (2,400 drops). There were about 8 - 12 drops standing between the edge of the core drop and the scintillator. One can see the simulated core drop in locations where there are no other drops, but once it falls behind the drop cloud it is reaching the point where it cannot be clearly discerned. In this small-drop case the core is more faintly discernible than it was in the case of large drops. The deep modulation caused by large drops obscures the core more quickly than does the more subtle modulation of small drops. Despite this fact, the core drop edges are highly corrupted and in fact the drop cloud edges in Figure 11b. are more prominent than the core drop edge. It would be impossible to separate drop cloud edge effects from core effects. Consistent with the effervescent spray results, x-ray PCI is incapable of imaging the larger structures inside a cloud of small drops

with fidelity, because the contribution of each drop persists within the x-ray beam. In both cases somewhere between 6 and 12 drop interactions is enough to obscure a liquid core. More importantly, just a few drops can corrupt the image of the core. The idea of extending *D* was again evaluated but it made no difference.

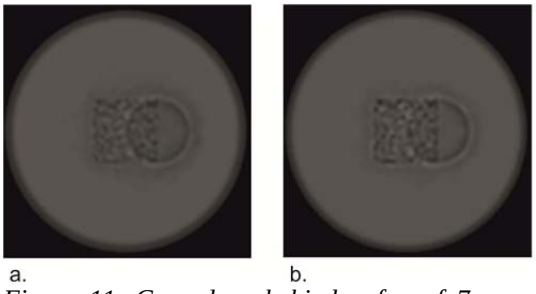

Figure 11. Core drop behind a fog of 7 μm drops.

Moon et al. [19] present x-ray phase contrast images of "near-nozzle jet morphology" from a hydroground single-hole Diesel injector using biodiesel (there are a number of similar reports [11, 15, 17]; this example was chosen for discussion here). An example image is presented in Figure 12a. One thing is immediately clear; it looks much more like a normal fluid stream than the x-ray PCI images discussed so far. The wording in the references provided can be understood to mean that the authors have successfully imaged an intact liquid core buried inside a dense spray, with very high spatial resolution and with very high dynamic range. Note that the quoted spatial resolution in Figure 12a. is 1 μm. Such high resolution should be able to detect any drops that might have been formed. It would in fact be impossible to avoid detection of such drops as we have already shown. The simulations presented earlier in this article have also demonstrated conclusively that it is not possible to image cleanly a liquid core inside a cloud of drops using x-ray PCI. An alternative explanation is required. Biodiesel has higher viscosity (up to two times higher) and surface tension (roughly 6% higher) than normal Diesel fuel; it would not break up as readily as Diesel fuel especially at moderate gas pressure. The hydroground nozzle also reduces the tendency to break up because it eliminates cavitation and minimizes turbulence inside the nozzle. In fact, if one looks closely at Figure 12a. one can see a flat edge to the flowfield on the top and bottom, indicating a laminar shear layer with the gas. Most of the image depicts a fully intact laminar but unsteady flow. The wave structure in the interior must be the development of an instability that finally transitions to turbulence much further downstream [25]. This is not what the core of an atomizing spray would look like. This evidence leaves just one reasonable conclusion; by design there were a negligible number of drops in the flow that produced Figure 12a. Such images cannot have been taken from an atomizing spray; on the contrary, they are images of a flow stream wherein the formation of drops has been suppressed. The question then is whether or not x-ray phase contrast images provide any more information about the actual mechanics of spray breakup than a good quality white light shadowgram like the one shown in Figure 12b. [25] does.

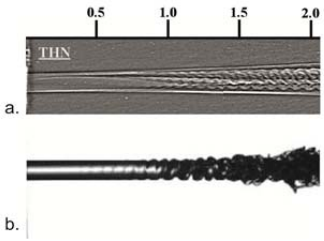

Figure 12. Comparison of x-ray PCI [20] with optical shadowgraphy [26].

These results were recently presented at ILASS-Americas [26]. Criticism of the work from the APS included: 1) The simulated synchrotron beam is highly idealized. The real beam is not collimated (it diverges somewhat) and it can include several harmonics (much broader bandwidth), 2) The modeled sprays are very dense, much denser than the sprays studied by the APS, and 3) The actual system has the scintillator moved in *closer* to the spray, not away from it. In response, it is easy to acknowledge that the simulation does not match all of the experimental realities because there is a serious lack of detailed information about the experiments in the literature, despite an extensive publication list. With respect to criticism 1), these beam details would certainly change the appearance of the simulated images somewhat (similar to the bandwidth issue already mentioned) but they would not change the conclusions. With respect to spray density (point number 2), there are very few measurements of drop size and volume fraction for this spray region in the literature, but if we take a known spray [27] and infer the number of drops one would expect for the spray in [15], it becomes clear that the simulated density is actually on the low side. Less dense sprays have also been modeled (e.g. Figure 7b) and those results make it clear that images of interior structures will be corrupted in the process, if not totally lost. Finally, moving the scintillator forward will first enhance images of small drops, not remove them. To move it even closer would corrupt both large and small structures (e.g. Fig. 4a and d). This is an interesting question, however, and so this case is currently being modeled (although the exact placement of the scintillator remains unknown to the author).

Summary and Conclusions

Simulations of X-ray phase contrast imaging have shown that X-ray PCI in sprays will produce complex patterns arising from drop clouds and that they cannot be interrogated. The results also make it clear that information about breakup mechanics of intact liquid structures buried inside a fully developed drop cloud of an atomizing spray cannot be extracted using X-ray PCI. It is this author's conclusion that phase contrast imaging cannot be used to study atomizing sprays unless there are very few droplets present. Under such conditions, existing optical methods (e.g. high speed shadowgraphy, planar imaging, holography and phase Doppler interferometry) can provide higher fidelity data at much lower cost.

Acknowledgements
The author is grateful to Dr. William Bachalo of Artium Technologies Inc. for very enlightening discussions, and to Dr. George Lawrence of AOR for insightful advice on the application of GLAD to this problem.

References

1. Blessing, M., et al. *SAE Technical Paper no. 2003-01-1358: Analysis of Flow and Cavitation Phenomena in Diesel Injection Nozzles and its Effects on Spray and Mixture Formation*. 2003.
2. Linne, M.A., et al., *Ballistic Imaging of Liquid Breakup Processes in Dense Sprays.* Proceedings of the Combustion Institute, 2009. **32**: p. 2147-2161.
3. MacPhee, A.G., et al., *X-ray imaging of shock waves generated by high-pressure fuel sprays.* Science, 2002. **295**: p. 1261-1263.
4. Cai, W., et al., *Quantitative analysis of highly transient fuel sprays by time-resolved x-radiography.* Applied Physics Letters, 2003. **83**(8): p. 1671-1673.
5. Renzi, M.J., et al., *Pixel array detectors for time resolved radiography.* Review of Scientific Instruments, 2002. **773**(3): p. 1621-1624.
6. EL-Hannouny, E.M., et al. *SAE Technical Paper Series, paper no. 2003-01-3150: Near-Nozzle Spray Characteristics of Heavy-Duty Diesel Injectors*. 2003.
7. Tanner, F.X., et al., *Structure of high-velocity dense sprays in the near-nozzle region.* Atomization and Sprays, 2006. **16**: p. 579–597.
8. Kastengren, A.L., et al. *SAE Technical Paper Series, paper no. 2007-01-0666: Determination of Diesel Spray Axial Velocity Using X-Ray Radiography*. 2007.
9. Kastengren, A.L., et al., *Measurement of Biodiesel Blend and Conventional Diesel Spray Structure Using X-Ray Radiography*. Journal of Engineering for Gas Turbines and Power, 2009. **131**.
10. Kastengren, A., et al. *SAE Technical Paper Series, paper no. 2011-01-0383: Correlation of Split-Injection Needle Lift and Spray Structure*. 2011.
11. Gao, J., et al., *Morphology of Diesel Sprays from Single-Orifice Micronozzles*, in *ILASS-Americas*. 2010: Cincinnati, OH.
12. Linne, M., *Detailed Numerical Analysis of X-ray Radiography in Sprays*, in *ICLASS - 12th International Conference on Liquid Atomization and Spray Systems*. 2012: Heidelberg, DE.
13. Wang, Y.J., et al., *Quantitative x-ray phase contrast imaging of air-assisted water sprays with high Weber numbers.* Applied Physics Letters, 2006. **89**.
14. Wang, Y., et al., *Ultrafast X-ray study of dense-liquid-jet flow dynamics using structure-tracking velocimetry.* Nature Physics, 2008. **4**: p. 305-309.
15. Liu, Z., et al., *Ultra-Fast Phase-Contrast X-ray Imaging of Near-Nozzle Velocity Field of High-Speed Diesel Fuel Sprays*, in *ILASS-Americas*. 2010: Cincinnati, OH.
16. Lai, M.-C., et al., *SAE Technical Paper Series, paper no. 2011-01-0681: Characterization of the Near-Field Spray and Internal Flow of Single-Hole and Multi-Hole Sac Nozzles using Phase Contrast X-Ray Imaging and CFD*. 2011.
17. Lai, M.-C., et al., *SAE Technical Paper Series, paper no. 2011-01-1881: Characterization of Internal flow and Spray of Multihole DI Gasoline Spray using X-ray Imaging and CFD*. 2011.
18. Lin, K.C., et al., *Exploration of Near-Field Structures of Aerated-Liquid Jets in a Quiescent Environment Using the X-Ray Technique*, in *ILASS-Americas*. 2010: Cincinnati, OH.
19. Moon, S., et al., *Ultrafast X-ray Phase-Contrast Imaging of High-Speed Fuel Sprays from a Two-Hole Diesel Nozzle*, in *ILASS-Americas*. 2010: Cincinnati, OH.
20. Gureyev, T.E., et al., *Refracting Röntgen's rays: Propagation-based x-ray phase contrast for biomedical imaging.* Journal of Applied Physics 2009. **105**.
21. Cloetens, P., et al., *Phase objects in synchrotron radiation hard x-ray imaging.* Journal of Physics D: Applied Physics, 1996. **29**: p. 133-146.
22. Lawrence, G.N., *GLAD Theory Manual, Ver. 5.5*. 2009.
23. Linne, M., *Analysis of X-ray phase contrast imaging in atomizing sprays.* Experiments in Fluids, 2012. **15**(5): p. 1201-1218.
24. Lasheras, J.C. and E.J. Hopfinger, *Liquid Jet Instability and Atomization in a Coaxial Gas Stream.* Annual Review of Fluid Mechanics, 2000. **32**: p. 275–308.
25. Balewski, B., *Experimental investigation of the influence of nozzle-flow properties on the primary spray breakup*, in *Mechanical Engineering*. 2009, Technical University of Darmstadt: Darmstadt, Germany.
26. Linne, M., *Detailed Numerical Analysis of X-ray Phase Contrast Imaging in Sprays*, in *ILASS-Americas*. 2012: San Antonio, TX.
27. Labs, J.E. and T.E. Parker, *Multiple-scattering effects on infrared scattering measurements used to characterize droplet size and volume fraction distributions in diesel sprays.* Applied Optics, 2005. **44**(28): p. 6049-6057.